

Rotational Quantum Beat Lasing Without Inversion

Maria Richter^{1,†,*}, Marianna Lytova^{2,†}, Felipe Morales¹, Stefan Haessler³, Olga Smirnova^{1,4}, Michael Spanner^{2,5}, & Misha Ivanov^{1,6,7}

¹*Max-Born-Institute, Max-Born Straße 2A, 12489 Berlin, Germany.*

²*Department of Physics, University of Ottawa, Ottawa K1N 6N5, Canada.*

³*Laboratoire d'Optique Appliquée, CNRS, École Polytechnique, ENSTA Paris, Institut Polytechnique de Paris, 181 Chemin de la Hunière et des Joncherettes, 91120 Palaiseau, France.*

⁴*Technische Universität Berlin, Ernst-Ruska-Gebäude, Hardenbergstraße 36A, 10623 Berlin, Germany.*

⁵*National Research Council of Canada, 100 Sussex Drive, Ottawa K1A 0R6, Canada.*

⁶*Department of Physics, Humboldt University, Newtonstraße 15, D-12489 Berlin, Germany.*

⁷*Blackett Laboratory, Imperial College London, SW7 2AZ London, United Kingdom.*

† These authors contributed equally, * Corresponding author

In standard lasers, light amplification requires population inversion between an upper and a lower state to break the reciprocity between absorption and stimulated emission. However, in a medium prepared in a specific superposition state, quantum interference may fully suppress absorption while leaving stimulated emission intact, opening the possibility of lasing without inversion. Here we show that lasing without inversion arises naturally during propagation of intense femtosecond laser pulses in air. It is triggered by the combination of

molecular ionization and molecular alignment, both unavoidable in intense light fields. The effect could enable inversionless amplification of broadband radiation in many molecular gases, opening unusual opportunities for remote sensing.

Introduction

A resonant light propagating through a medium will be absorbed by the medium in a lower state and will stimulate emission if the medium is excited. For a quantum system pumped into an excited state $|e\rangle$, with an empty state $|g\rangle$ below, population inversion between these two states leads to amplification of a probe light at the $|e\rangle \rightarrow |g\rangle$ transition frequency. For almost six decades, this process has been exploited in conventional lasers. However, already three decades ago, it has been shown that lasing can also occur without population inversion¹⁻⁸.

The basic idea behind lasing without inversion⁹⁻¹¹ (LWI) is similar to conventional lasers – to prepare a medium where emission is favored over absorption, so that resonant light is amplified as it propagates in the medium. The difference lies in the medium preparation. Instead of creating population inversion between the lasing states, quantum interference is used to suppress photo-absorption while keeping photo-emission intact. In the simplest scheme, two lower-lying states $|g_1\rangle$ and $|g_2\rangle$ are each coupled to a common upper state $|e_1\rangle$, see Fig.1(a). One can prepare a coherent superposition of the two lower states, such that the transition from this superposition to the upper state vanishes due to destructive interference of the transition amplitudes $|g_1\rangle \rightarrow |e_1\rangle$ and $|g_2\rangle \rightarrow |e_1\rangle$. Now, any population pumped incoherently into the upper state can provide gain.

A number of different schemes for lasing without inversion have been developed^{9,10}. Taking advantage of destructive interference of different pathways in absorption, they generally strive to maintain a specific phase relationship between the lower-lying states, which carry most of the population. Here we present a scheme that does not follow this tradition. It uses only the natural dynamics of a multi-level quantum system and requires no coherence between the excited and the lower electronic states; effectively, lasing without inversion comes 'for free'. We also show that this mechanism is active in the highly efficient generation of 391 nm radiation during propagation of intense femtosecond laser pulses in air¹²⁻¹⁶, under standard conditions where the process known as "laser filamentation"¹⁷⁻¹⁹ leads to self-guiding of light.

Identifying the mechanism responsible for this effect, commonly referred to as 'air lasing', has been a long-standing puzzle²⁰⁻⁴⁵. The main difficulty in resolving this puzzle stems from the apparent lack of a general physical mechanism capable of generating population inversion for the dominant observed amplification line around 391 nm, for standard filamentation conditions including the clamping of the laser intensity around $I \sim 10^{14}$ W/cm². The 391 nm line corresponds to the transition between the two ground vibrational levels $\nu'', \nu' = 0$ of the electronic states $X^2\Sigma_g^+$ (denoted as X) and $B^2\Sigma_u^+$ (denoted as B) in N_2^+ . We believe that our inversionless mechanism provides the key missing component of this puzzle. Compared to the recent proposal in Ref.³⁵, we fully account for the vibrational and rotational dynamics of the molecule; our lasing mechanism remains operative even in the absence of initial coherence between the ionic states.

Results and discussion

In its simplest form, our amplification mechanism can be referred to as rotational quantum beat lasing. It is illustrated in Fig.1(b)-(d), and can be easily understood in the time domain. When an intense femtosecond laser pulse interacts with a diatomic molecule, or its ion, it induces molecular alignment^{46,47}. This alignment revives periodically after the pulse is gone, Fig.1(b). The revival dynamics demonstrates a sequence of alignment and anti-alignment with the revival period controlled by the rotational constant B_0 . Fig.1(b) shows the evolution of the characteristic alignment measure, $\langle \cos^2 \theta \rangle(t)$, for a nitrogen molecule at room temperature (298 K), after interacting with a 23 fs FWHM, 800 nm pump pulse with a peak intensity of 10^{14} W/cm² (see Methods). Its minima correspond to anti-alignment, its maxima to maximum alignment with the direction of the linearly polarized, aligning laser field.

Suppose now that similar rotational dynamics is induced in two electronic (vibronic) states, $|1\rangle$ and $|2\rangle$, with a dipole-allowed electronic transition between them. In diatomics, electronic transitions can be either parallel or perpendicular to the molecular axis; for definiteness, let this transition be parallel. Its probability is then proportional to $\cos^2 \theta$, where θ is the angle between the molecular axis and the laser electric field inducing the transition. For a molecule rotating in the lower vibronic state, the probability of parallel absorption $|1\rangle \rightarrow |2\rangle$ thus depends on $\langle \cos^2 \theta \rangle_1(t)$ averaged over the rotational dynamics in state $|1\rangle$, which is controlled by its rotational constant B_0^1 . Conversely, for a molecule rotating in the upper vibronic state $|2\rangle$, the emission probability $|2\rangle \rightarrow |1\rangle$ depends on $\langle \cos^2 \theta \rangle_2(t)$, with its time-dependence controlled by B_0^2 .

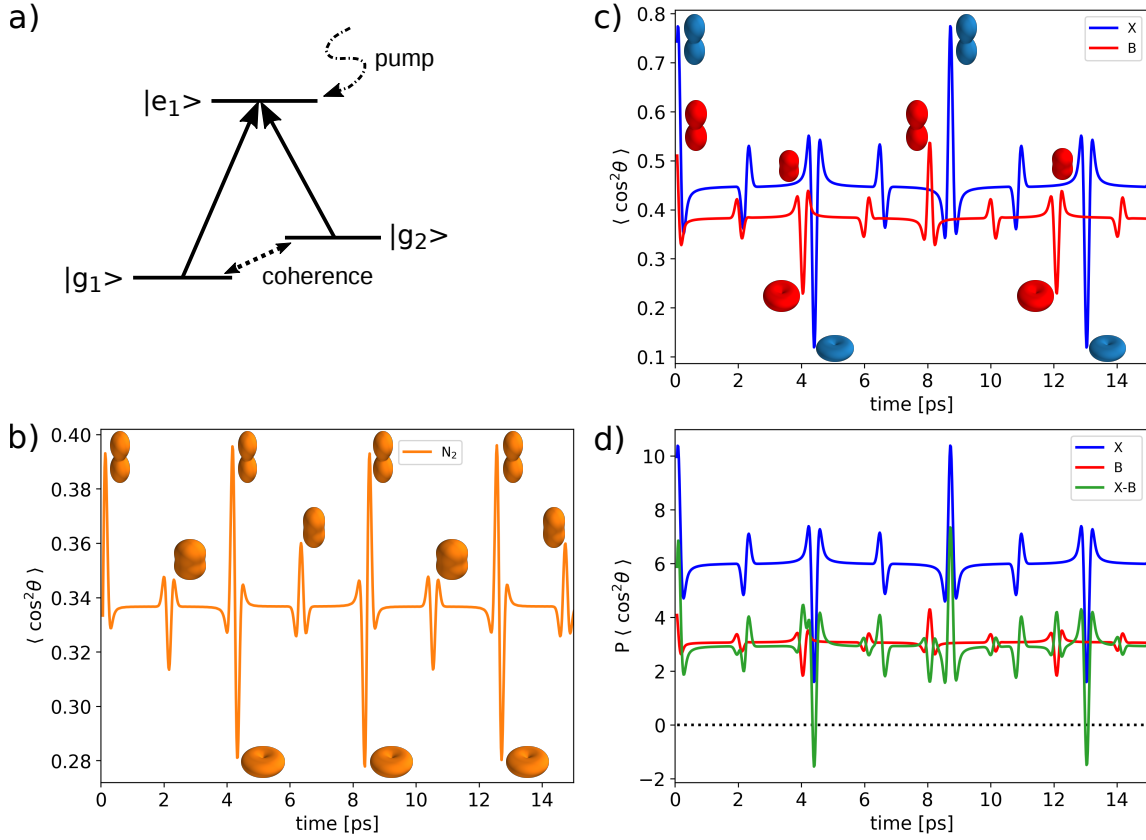


Figure 1: Schematic of a rotational quantum beat laser without inversion in the time domain using the example of N_2^+ . Calculations are performed for a 23 fs, 800 nm, 10^{14} W/cm² pump pulse and room temperature (298 K). The 3D shapes in (b,c) sketch the angular distributions of the rotating molecular ensembles. (a) Conventional lasing-without-inversion gain medium with low-frequency coherence between a pair of states. (b) Molecular alignment of N_2 at 298 K induced by the intense femtosecond pump pulse. (c) Rotational dynamics in the two vibronic states $|X, \nu'' = 0\rangle$ and $|B, \nu' = 0\rangle$ of N_2^+ induced by the same pump. (d) Gain windows (at $\tau_1 \simeq 4.3$ ps and $\tau_2 \simeq 13.0$ ps) without population inversion at a parallel transition between the two vibronic states are enabled by the different angular distribution geometries of the rotating molecular ensembles in the upper and the lower states; no coherence between the two rotational manifolds is required.

Opportunities for inversionless amplification of a short probe pulse, polarized parallel to the pump and delayed by τ , arise when the $|1\rangle$ state molecules are anti-aligned, so that $\langle \cos^2 \theta \rangle_1(\tau)$ is minimum and the parallel $|1\rangle \rightarrow |2\rangle$ absorption is suppressed. This opportunity is further enhanced if the $|2\rangle$ state molecules are aligned at this time, so that $\langle \cos^2 \theta \rangle_2(\tau)$ is maximum and the parallel $|2\rangle \rightarrow |1\rangle$ emission is enhanced. This possibility to use molecular alignment for inversionless amplification was previously pointed out by A. K. Popov and V. V. Slabko⁴⁸. The converse is true if the $|1\rangle$ state molecules are aligned when the probe pulse arrives, while the $|2\rangle$ state molecules are anti-aligned, enhancing absorption. As long as B_0^1 and B_0^2 are different, the two rotations will go out of sync, arriving at the point where the lower state is anti-aligned and the upper is still aligned and vice versa (Fig 1c). Overall, temporal windows of gain will be followed by windows of loss, leading to the rotational quantum beats in the time-resolved gain-loss of the short probe pulse.

Figs.1(c,d) give the specific example. Fig.1(c) shows the rotational dynamics in the two ground vibrational levels $\nu'', \nu' = 0$ of the electronic states X and B in N_2^+ , induced by the same pump pulse interacting with N_2 , Fig.1(b). The short pump pulse impulsively aligns the neutral N_2 molecules, generating the rotational dynamics in Fig.1(b). It also ionizes some of the N_2 molecules, producing molecular ions predominantly in the ground X , but also in the excited A ($A^2\Pi_u$) and B states, and continues to align them. After the end of the pulse, the ions continue to rotate, reaching maximum alignment at $t \simeq 90$ fs for the X and B states, see Fig.1(c), followed by periodic revivals of alignment and anti-alignment. They correspond to maxima and minima in the rotational ensemble-averaged $\langle \cos^2 \theta \rangle_{X,B}(t)$, where subscripts denote the ionic states (see Methods). These revivals are different due to slight differences in the rotational constants $B_0^{X,B}$.

Frequency-integrated absorption at the parallel $|X, \nu'' = 0\rangle \rightarrow |B, \nu' = 0\rangle$ transition behaves as $W_{\text{abs}}(\tau) \propto P_X \langle \cos^2 \theta \rangle_X(\tau)$, where P_X is the $|X, \nu'' = 0\rangle$ -state population (see Methods). In emission, $W_e(\tau) \propto P_B \langle \cos^2 \theta \rangle_B(\tau)$. Gain windows open when $P_B \langle \cos^2 \theta \rangle_B(\tau) > P_X \langle \cos^2 \theta \rangle_X(\tau)$, see Fig.1(d). The populations of the X and B states, $P_{X,B}$, determine the length and the strength of the gain windows, however, overall electronic population inversion is not needed, Fig.1(d). Comprehensive quantitative analysis presented below shows that this naturally arising amplification mechanism does indeed lead to gain at the rotational frequency band around 391 nm during filamentation of intense femtosecond laser pulses in air or N_2 gas, including the intensity regime $I \lesssim 10^{14} \text{ W/cm}^2$ pertinent to laser filamentation.

Most experiments studying this effect^{14, 20–22, 24, 26, 27, 30–32, 34–39, 41–44} are done in a pump-probe scenario: an intense pump pulse prepares the gas and transient absorption (or gain) of a delayed probe pulse is measured. The theoretical results presented below focus on this scenario, with the pump pulse carried at 800 nm. Details are given in the Methods section, here we outline key issues requiring particular attention when addressing this rather challenging problem quantitatively.

Our theoretical description accounts for laser-induced alignment of the neutral N_2 molecule, its alignment-dependent strong-field ionization into the laser-dressed states of the molecular ion, and full laser-induced electronic, vibrational and rotational dynamics in the ion involving the X, A, B states. Our ab-initio simulations of strong-field ionization use the method of Ref.⁴⁹, and allow us to evaluate the excitation of the different ionic states induced by the recollision of the photoelectron with the parent ion in the X state^{23, 24, 33–35, 40}. The role of recollision is gauged by

absorbing the electron wavepacket before it is turned around towards the parent ion. Eliminating the recollision reduces the population of the B state by about 1%, compared to the case when the recollision is included. Thus, the recollision can be neglected and the photo-electron can be integrated out. Here, one must account for the electron-ion entanglement. Since the X and B states have opposite parity, the photo-electron wavepackets correlated to them will also carry opposite parity, remaining orthogonal to each other. This eliminates the coherence between the X and B states that could have been produced during strong-field ionization.

Regarding optical $X \rightarrow B$ excitation by an 800 nm pump, the $|X, \nu'' = 0\rangle \rightarrow |B, \nu' = 0\rangle$ transition corresponds to absorption of two photons, which is parity forbidden; noticeable excitation is only generated at very high intensities, $I \gtrsim 4 \times 10^{14}$ W/cm² (the domain of several recent pump-probe experiments but not relevant for standard laser filamentation conditions), when the system is strongly distorted and higher-order multiphoton transitions can occur. In this context, note that strong-field ionization populates not field-free^{25,41,42,45,50} but already polarized (dressed by the field) ionic X , A , and B states. Indeed optical tunneling results from polarization of the many-body wave function of the neutral as one of the polarized electrons leaks through the potential barrier, leaving other electrons polarized. Comparison to ab-initio simulations⁴⁹ show that initializing population in the field-free ionic states at the peaks of the instantaneous electric field, where strong-field ionization takes place, generates spurious excitations of the A and B states due to effectively abrupt turn-on of the laser-ion interaction.

Moreover, the initial thermal rotational distribution must be included. Each rotational state

in the initial thermal distribution gives rise to a rotational wavepacket induced by the pump. Each wavepacket leads to coherent effects in emission and absorption; these contributions are added incoherently with the corresponding weights.

With these aspects accounted for, our calculations reveal a robust physical mechanism leading to gain at the 391 nm line. In contrast to Ref.³⁵, it does not require the coherence between the X and B states, and is based on the mechanism described in Fig.1.

In the frequency domain, the rotational quantum beat mechanism can be understood as follows. The short, intense pump pulse aligning and ionizing the N_2 molecules, generates broad rotational distributions in the X and B states of N_2^+ , with coherent population of many adjacent rotational states with similar amplitudes in each electronic state. Fig.2(a) shows the rotational distributions in $|X, \nu'' = 0\rangle$ and $|B, \nu' = 0\rangle$ for the case of the 800 nm, 23 fs FWHM pump pulse with an intensity of $I = 10^{14}$ W/cm² and the N_2 molecules initially at room temperature (298 K).

Consider now frequency-resolved transient absorption of a short probe pulse at the dipole-allowed transition $|X, J\rangle \rightarrow |B, J + 1\rangle$ (with the vibrational quantum number equal to zero in both cases). For each initial rotational state of the neutral, rotational coherence generated in the X state of the ion means that the absorption $|X, J\rangle \rightarrow |B, J + 1\rangle$, stimulated by a broadband probe, is inevitably accompanied by the absorption $|X, J + 2\rangle \rightarrow |B, J + 1\rangle$ stimulated by the same probe, Fig.2(b). Their interference is governed by the relative phase between the two lower states, $\phi_X(J + 2, J)(t) = \Delta E_X(J + 2, J)t + \phi_X^{(0)}(J, J + 2)$. Here $\Delta E_X(J + 2, J) = B_0^X [(J + 2)(J + 3) - J(J + 1)]$ is the distance between the two states in X and $\phi_X^{(0)}$ is their re-

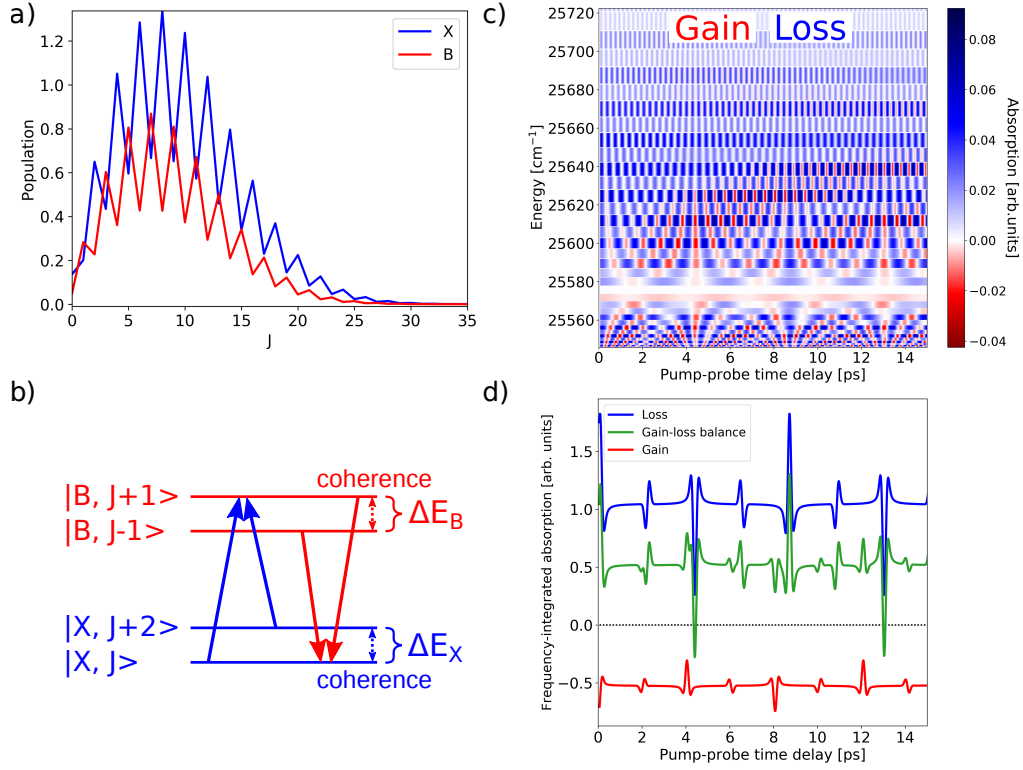


Figure 2: Rotational quantum beat lasing without inversion in the frequency domain using the example of N_2^+ . Calculations are performed for the same pump pulse and temperature as in Fig.1 and a 20 fs, 391 nm, 10^{11} W/cm² probe pulse. (a) Rotational distributions in the X and B states of N_2^+ formed at the end of the interaction with the intense femtosecond pump pulse. (b) Four-level system controlling absorption and emission at the $|X, J\rangle \rightarrow |B, J+1\rangle$ transition. (c) Full simulation of the frequency-resolved gain (red) and loss (blue) of the weak probe interacting with the pumped system as a function of pump-probe delay. (d) Absorption (blue) and emission (negative absorption) (red) integrated over all frequencies follow the alignment dynamics in Fig.1(c,d). The total gain-loss balance integrated over all frequencies (green) follows the pattern of $P_X \langle \cos^2 \theta \rangle_X - P_B \langle \cos^2 \theta \rangle_B$ in Fig.1(d), showing the same gain windows for the inversionless medium ($P_X > P_B$).

lative phase at the start of the field-free evolution when the pump is over. Destructive interference between the $|X, J\rangle \rightarrow |B, J + 1\rangle$ and $|X, J + 2\rangle \rightarrow |B, J + 1\rangle$ transitions occurs when $\phi_X(J + 2, J)(t) = (2N \pm 1)\pi$ (N is integer), resulting in suppression of absorption of a short probe pulse arriving at this moment. Conversely, constructive interference enhances absorption when $\phi_X(J + 2, J)(t) = 2N\pi$. This leads to the quantum beat in the time-dependent absorption rate of the short probe pulse with frequency $\Delta E_X(J + 2, J)$.

Emission at the same frequency, $|B, J + 1\rangle \rightarrow |X, J\rangle$, is inevitably accompanied by the transition $|B, J - 1\rangle \rightarrow |X, J\rangle$, Fig.2(b). Their interference is governed by the relative phase $\phi_B(J + 1, J - 1)(t) = \Delta E_B(J + 1, J - 1)t + \phi_B^{(0)}(J - 1, J + 1)$ with $\Delta E_B(J + 1, J - 1) = B_0^B [(J + 1)(J + 2) - (J - 1)J]$. Constructive interference between $|B, J + 1\rangle \rightarrow |X, J\rangle$ and $|B, J - 1\rangle \rightarrow |X, J\rangle$ in emission occurs when $\phi_B(J + 1, J - 1)(t) = 2N\pi$, while destructive interference occurs when $\phi_B(J + 1, J - 1)(t) = (2N \pm 1)\pi$, leading to the quantum beat in the time-dependent emission rate with frequency $\Delta E_B(J + 1, J - 1)$.

The difference between the rotational constants B_0^X and B_0^B means that there are time-windows where destructive interference of the $|X, J\rangle \rightarrow |B, J + 1\rangle$ and $|X, J + 2\rangle \rightarrow |B, J + 1\rangle$ transitions in absorption (when $\phi_X(J + 2, J)(t) = (2N \pm 1)\pi$) coincides with constructive interference of the $|B, J + 1\rangle \rightarrow |X, J\rangle$ and $|B, J - 1\rangle \rightarrow |X, J\rangle$ transitions in emission (when $\phi_B(J + 1, J - 1)(t) = 2N\pi$). This leads to frequency-resolved (J -dependent) gain and loss windows as a function of the pump-probe time-delay, shown in Fig.2(c) for a weak 20 fs Gaussian probe pulse with a central wavelength of 391 nm.

As many four-level systems such as the one shown in Fig.2(b) are formed by the pump, they generate a rich gain (red)-loss (blue) pattern of frequency-resolved transient absorption of the probe pulse, see Fig.2(c). Each vertical line shows the frequency-resolved absorption for a particular pump-probe time delay, integrated over the full duration of the probe pulse. The horizontal white line around $\tilde{\nu} \simeq 25575 \text{ cm}^{-1}$ marks the energy spacing $\tilde{\nu}_{00}$ between the two ground ro-vibrational levels of the electronic states X and B . The spectral lines above this energy are associated with the higher-energy branch (R branch). Those below 25575 cm^{-1} to the lower energy branch (P branch).

Time-dependent gain emerges for virtually all pump-probe time delays and many transition frequencies, especially those associated with the lower-energy P-branch. Most notably, for those time delays at which the X state molecules are anti-aligned with the probe polarization direction, e.g. around $\tau \simeq 4.3 \text{ ps}$, amplification occurs across the whole range of frequencies. Fig.2(c) incorporates the comprehensive modeling of the whole process, starting with the thermal ensemble of neutral molecules and accounting for (i) alignment of the neutral molecule, (ii) its angle-dependent strong-field ionization into the laser-dressed ionic states, with the ratio of B to X state populations at 20% upon ionization, (iii) entanglement between the photo-electron and the ion, which negates the X - B coherence once the photo-electron is integrated out, (iv) coupled electronic, vibrational, and rotational dynamics in the ion, and (v) comprehensive calculations of transient absorption and emission of the probe pulse including all interferences. Note that gain windows emerge with neither electronic nor rotational population inversion, Fig.2(a).

Fig.2(d) connects the frequency-domain picture of Fig.2(c) to the time-domain picture of

Figs.1(c,d). It shows the frequency-integrated absorption from the X state (blue line) and emission (negative absorption) from the B state (red line) stimulated by the short probe pulse, as a function of the pump-probe delay. The pattern of each line follows the alignment measure of the respective ion in Fig.1(c). This is not a coincidence. The same phase differences that control the interferences in transient absorption by each $(|X, J\rangle, |X, J+2\rangle)$ pair, control their contribution to the ensemble-averaged $\langle \cos^2 \theta \rangle_X$ measure of the field-free rotations in the X state. The same applies to emission by each $(|B, J-1\rangle, |B, J+1\rangle)$ pair and the ensemble-averaged $\langle \cos^2 \theta \rangle_B$ measure. As shown in Methods, integrating the frequency-resolved absorption over all frequencies yields the total transient absorption probability $W_{\text{abs}}(\tau) \propto P_X \langle \cos^2(\theta) \rangle_X(\tau)$. Analogous results hold for transient emission.

The green line in Fig.2(d) shows the overall gain-loss balance, integrated over all energies. As expected, the strongest gain windows coincide with anti-alignment of the X state, cf. Fig.1(c,d), when the gain-loss pattern in Fig.2(c) shows gain across the whole spectrum. If the X and B state molecules would anti-align simultaneously during their field-free evolution, the net gain would vanish.

Results presented in Fig.2 are robust with respect to the pump parameters, and the lasing mechanism described above is completely general. The only necessary ingredients are non-negligible population in the B state and molecular rotations, both unavoidable during the interaction with an intense laser pulse. For the pump pulse parameters and temperature used for Figs.1,2, our simulations show that net gain sets in already at the ratio $P_B/P_X \simeq 10\%$ upon ionization.

Fig.3 shows results for two other pump intensities realistic in laser filamentation. The expected "clamping" intensity is $I \lesssim 1 \times 10^{14} \text{ W/cm}^2$, but pulse compression during filamentation suggests that short intensity spikes can reach^{51,52} $I \sim 2 \times 10^{14} \text{ W/cm}^2$. For 800 nm driver fields with intensities $I \lesssim 2 \times 10^{14} \text{ W/cm}^2$, the B state population is not strongly affected by laser-driven excitations from X . However, the higher the intensity, the stronger the depletion of the X state into A ^{25,26} (especially for pump pulses shorter or comparable to the ~ 18 fs vibrational period in the A state), yielding an overall change of the gain-loss balance in favor of gain and hence the emergence of additional gain windows in time, Figs.3(d).

The results presented in Fig.3 are in remarkably good agreement with recent experimental findings^{38,39}. Ref.³⁸ reports on pump-probe femtosecond filamentation experiments in a nitrogen gas cell, measuring the delay-dependent amplification of the probe around the 391 nm line using a high-resolution spectrometer. Our simulations closely reproduce all the main features of the measured time- and frequency-resolved gain, including the parabolic structure of the gain, the fast temporal modulation of each rotational line that increases with J in the R branch, and the slower temporal modulation, reflecting the molecular alignment dynamics and giving rise to the distinct gain window at $\tau \sim 4.3$ fs where amplification occurs across the whole spectrum. Experiments that do not resolve each individual rotational line observe (the weighted sum of) frequency window-integrated, highly oscillating gain-loss structures, such as the ones shown in Figs.3(b,d). For increasing pump intensity, the oscillating gain starts to occur for virtually all pump-probe time delays, as observed in the nitrogen gas jet experiments in Ref.³⁹.

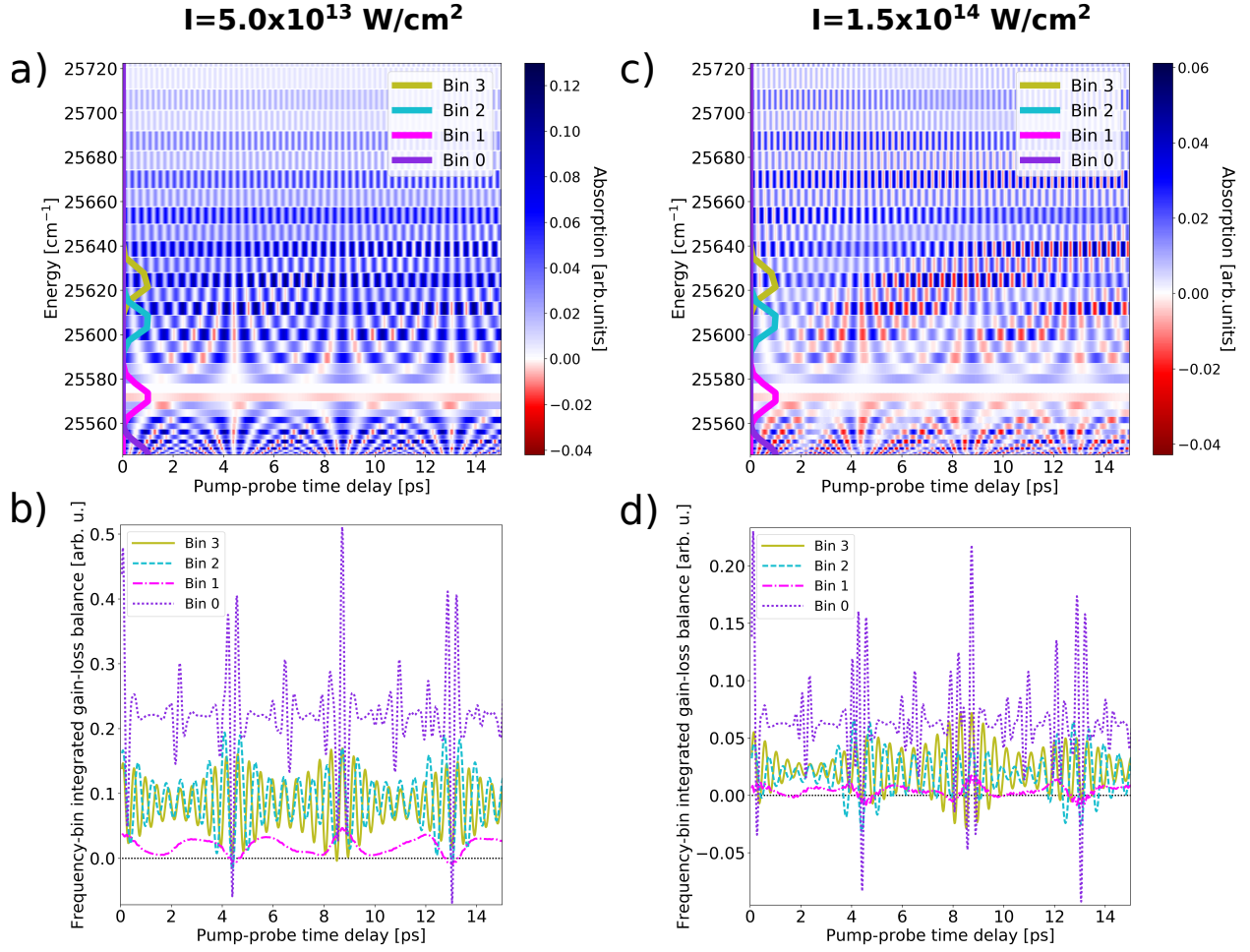


Figure 3: Rotational quantum beat lasing in N_2^+ for different intensities realistic in femtosecond laser filamentation experiments. Calculations are performed for a 23 fs, 800 nm pump pulse and the same probe pulse and temperature as in Fig.2. (a,c) Same as Fig.2(c), but for a pump intensity of (a) $I = 5.0 \times 10^{13} \text{ W/cm}^2$ and (c) $I = 1.5 \times 10^{14} \text{ W/cm}^2$. (b,d) Gain-loss balance integrated over the frequency windows (bins) indicated in panels (a,c). For both intensities, gain windows emerge without population inversion of the medium ($P_X > P_B$) (Gain windows also emerge for the total gain-loss balance integrated over all frequencies, analog to Fig.2d).

In the present mechanism, the gain window travels with the group velocity of the pump pulse, so that amplification occurs only in the forward direction. To achieve lasing in the backward direction, highly desirable for remote sensing, one would greatly benefit from creating population inversion, at least between the rotational states. To this end, a sequence of two well-timed pump pulses can be used to control rotations of X and B states of the ion. Their different rotational periods mean that the second pulse can be timed to simultaneously accelerate rotations of the B -state and slow down the rotations of the X state, generating rotational inversion. Optimization of such pulse sequence, including their carrier frequencies, energies, and time-delay, should open a route for achieving robust and strong backward lasing in open air.

Acknowledgements

We acknowledge many fruitful and stimulating discussions with Daniil Kartashov, Andrius Baltuška, Mathew Britton and Paul Corkum. M.I. acknowledges support from the Deutsche Forschungsgemeinschaft (DFG) Quantum Dynamics in Tailored Intense Fields (QUTIF) grant no. IV 152/6-1, and from the Engineering and Physical Sciences Research Council/Defence Science and Technology Laboratory (EPSRC/DSTL) Multidisciplinary University Research Initiative (MURI) grant no. EP/N018680/1. O.S. acknowledges support from the DFG Schwerpunktprogramm 1840 Quantum Dynamics in Tailored Intense Fields project SM 292/5-1, and Molecular Electron Dynamics Investigated by Intense Fields and from the Attosecond Pulses (MEDEA) project, which has received funding from the European Unions Horizon 2020 research and innovation programme under the Marie Skłodowska-Curie grant agreement no. 641789. S.H. acknowledges support from

REFERENCES

the Laboratoire d'Excellence Physique: Atomes Lumière Matière (LabEx PALM) overseen by the Agence Nationale pour la Recherche as part of the Investissements d'Avenir program (ANR-10-LABX-0039).

REFERENCES

References

1. Kocharovskaya, O. A. & Khanin, Y. I. Coherent amplification of an ultrashort pulse in a three-level medium without a population inversion. Pis'ma Zh. Eksp. Teor. Fiz. **48**, 581 (1988) [*JETP Lett.* **48**, 630 - 634 (1988)].
2. Khanin, Y. I. & Kocharovskaya, O. A. Inversionless amplification of ultrashort pulses and coherent population trapping in a three-level medium. J. Opt. Soc. Am. B **7**, 2016–2024 (1990). URL <http://josab.osa.org/abstract.cfm?URI=josab-7-10-2016>.
3. Scully, M. O., Zhu, S.-Y. & Gavrielides, A. Degenerate quantum-beat laser: Lasing without inversion and inversion without lasing. Phys. Rev. Lett. **62**, 2813–2816 (1989). URL <https://link.aps.org/doi/10.1103/PhysRevLett.62.2813>.
4. Harris, S. E. Lasers without inversion: Interference of lifetime-broadened resonances. Phys. Rev. Lett. **62**, 1033–1036 (1989). URL <https://link.aps.org/doi/10.1103/PhysRevLett.62.1033>.
5. Nottelmann, A., Peters, C. & Lange, W. Inversionless amplification of picosecond pulses due to zeeman coherence. Phys. Rev. Lett. **70**, 1783–1786 (1993). URL <https://link.aps.org/doi/10.1103/PhysRevLett.70.1783>.

REFERENCES

REFERENCES

6. Fry, E. S. et al. Atomic coherence effects within the sodium d_1 line: Lasing without inversion via population trapping. Phys. Rev. Lett. **70**, 3235–3238 (1993). URL <https://link.aps.org/doi/10.1103/PhysRevLett.70.3235>.
7. van der Veer, W. E., van Diest, R. J. J., Dönszelmann, A. & van Linden van den Heuvell, H. B. Experimental demonstration of light amplification without population inversion. Phys. Rev. Lett. **70**, 3243–3246 (1993). URL <https://link.aps.org/doi/10.1103/PhysRevLett.70.3243>.
8. Zibrov, A. S. et al. Experimental demonstration of laser oscillation without population inversion via quantum interference in Rb. Phys. Rev. Lett. **75**, 1499–1502 (1995). URL <https://link.aps.org/doi/10.1103/PhysRevLett.75.1499>.
9. Kocharovskaya, O. Amplification and lasing without inversion. Physics Reports **219**, 175–190 (1992). URL <http://www.sciencedirect.com/science/article/pii/037015739290135M>.
10. Scully, M. O. From lasers and masers to phaseonium and phasers. Physics Reports **219**, 191–201 (1992). URL <http://www.sciencedirect.com/science/article/pii/037015739290136N>.
11. Scully, M. O. & Fleischhauer, M. Lasers without inversion. Science **263**, 337–338 (1994). URL <https://science.sciencemag.org/content/263/5145/337>. <https://science.sciencemag.org/content/263/5145/337.full.pdf>.

REFERENCES

REFERENCES

12. Luo, Q., Liu, W. & Chin, S. Lasing action in air induced by ultra-fast laser filamentation. Applied Physics B **76**, 337–340 (2003). URL <https://doi.org/10.1007/s00340-003-1115-9>.
13. Yao, J. et al. High-brightness switchable multiwavelength remote laser in air. Phys. Rev. A **84**, 051802 (2011). URL <https://link.aps.org/doi/10.1103/PhysRevA.84.051802>.
14. Yao, J. et al. Remote creation of coherent emissions in air with two-color ultrafast laser pulses. New Journal of Physics **15**, 023046 (2013). URL <https://doi.org/10.1088/1367-2630/15/2/023046>.
15. Liu, Y., Brelet, Y., Point, G., Houard, A. & Mysyrowicz, A. Self-seeded lasing in ionized air pumped by 800 nm femtosecond laser pulses. Opt. Express **21**, 22791–22798 (2013). URL <http://www.opticsexpress.org/abstract.cfm?URI=oe-21-19-22791>.
16. Chu, W. et al. A self-induced white light seeding laser in a femtosecond laser filament. Laser Physics Letters **11**, 015301 (2013). URL <https://doi.org/10.1088/2F1612-2011%2F11%2F1%2F015301>.
17. Braun, A. et al. Self-channeling of high-peak-power femtosecond laser pulses in air. Opt. Lett. **20**, 73–75 (1995). URL <http://ol.osa.org/abstract.cfm?URI=ol-20-1-73>.
18. Couairon, A. & Mysyrowicz, A. Femtosecond filamentation in transparent media. Physics Reports **441**, 47 – 189 (2007). URL <http://www.sciencedirect.com/science/article/pii/S037015730700021X>.

REFERENCES

REFERENCES

19. Bergé, L., Skupin, S., Nuter, R., Kasparian, J. & Wolf, J.-P. Ultrashort filaments of light in weakly ionized, optically transparent media. Reports on Progress in Physics **70**, 1633–1713 (2007). URL <https://doi.org/10.1088%2F0034-4885%2F70%2F10%2Fr03>.
20. Ni, J. et al. Identification of the physical mechanism of generation of coherent N_2^+ emissions in air by femtosecond laser excitation. Opt. Express **21**, 8746–8752 (2013). URL <http://www.opticsexpress.org/abstract.cfm?URI=oe-21-7-8746>.
21. Zhang, H. et al. Rotational coherence encoded in an “air-laser” spectrum of nitrogen molecular ions in an intense laser field. Phys. Rev. X **3**, 041009 (2013). URL <https://link.aps.org/doi/10.1103/PhysRevX.3.041009>.
22. Li, G. et al. Signature of superradiance from a nitrogen-gas plasma channel produced by strong-field ionization. Phys. Rev. A **89**, 033833 (2014). URL <https://link.aps.org/doi/10.1103/PhysRevA.89.033833>.
23. Mitryukovskiy, S. et al. Plasma luminescence from femtosecond filaments in air: Evidence for impact excitation with circularly polarized light pulses. Phys. Rev. Lett. **114**, 063003 (2015). URL <https://link.aps.org/doi/10.1103/PhysRevLett.114.063003>.
24. Liu, Y. et al. Recollision-induced superradiance of ionized nitrogen molecules. Phys. Rev. Lett. **115**, 133203 (2015). URL <https://link.aps.org/doi/10.1103/PhysRevLett.115.133203>.

REFERENCES

REFERENCES

25. Xu, H., Lötstedt, E., Iwasaki, A. & Yamanouchi, K. Sub-10-fs population inversion in N_2^+ in air lasing through multiple state coupling. Nature Communications **6**, 8347 (2015). URL <https://doi.org/10.1038/ncomms9347>.
26. Yao, J. et al. Population redistribution among multiple electronic states of molecular nitrogen ions in strong laser fields. Phys. Rev. Lett. **116**, 143007 (2016). URL <https://link.aps.org/doi/10.1103/PhysRevLett.116.143007>.
27. Kartashov, D. et al. Transient inversion in rotationally aligned nitrogen ions in a femtosecond filament. In Research in Optical Sciences, HTh4B.5 (Optical Society of America, 2014). URL <http://www.osapublishing.org/abstract.cfm?URI=HILAS-2014-HTh4B.5>.
28. Richter, M., Morales, F., Spanner, M., Smirnova, O. & Ivanov, M. Optical lasing during laser filamentation in the nitrogen molecular ion: Ro-vibrational inversion. In 2017 Conference on Lasers and Electro-Optics Europe European Quantum Electronics Conference (CLEO/Europe-EQEC), 1–1 (2017).
29. Azarm, A., Corkum, P. & Polynkin, P. Optical gain in rotationally excited nitrogen molecular ions. Phys. Rev. A **96**, 051401 (2017). URL <https://link.aps.org/doi/10.1103/PhysRevA.96.051401>.
30. Lei, M., Wu, C., Zhang, A., Gong, Q. & Jiang, H. Population inversion in the rotational levels of the superradiant N_2^+ pumped by femtosecond laser pulses. Opt. Express

REFERENCES

REFERENCES

- 25**, 4535–4541 (2017). URL <http://www.opticsexpress.org/abstract.cfm?URI=oe-25-4-4535>.
31. Zhong, X. et al. Vibrational and electronic excitation of ionized nitrogen molecules in intense laser fields. Phys. Rev. A **96**, 043422 (2017). URL <https://link.aps.org/doi/10.1103/PhysRevA.96.043422>.
32. Xu, H., Lötstedt, E., Ando, T., Iwasaki, A. & Yamanouchi, K. Alignment-dependent population inversion in N_2^+ in intense few-cycle laser fields. Phys. Rev. A **96**, 041401 (2017). URL <https://link.aps.org/doi/10.1103/PhysRevA.96.041401>.
33. Liu, Y. et al. Unexpected sensitivity of nitrogen ions superradiant emission on pump laser wavelength and duration. Phys. Rev. Lett. **119**, 203205 (2017). URL <https://link.aps.org/doi/10.1103/PhysRevLett.119.203205>.
34. Britton, M. et al. Testing the role of recollision in N_2^+ air lasing. Phys. Rev. Lett. **120**, 133208 (2018). URL <https://link.aps.org/doi/10.1103/PhysRevLett.120.133208>.
35. Mysyrowicz, A. et al. Lasing without population inversion in N_2^+ . APL Photonics **4**, 110807 (2019). URL <https://doi.org/10.1063/1.5116898>.
36. Xu, B. et al. Free-space N_2^+ lasers generated in strong laser fields: the role of molecular vibration. Opt. Express **26**, 13331–13339 (2018). URL <http://www.opticsexpress.org/abstract.cfm?URI=oe-26-10-13331>.

REFERENCES

REFERENCES

37. Zhong, X. et al. Optimizing the 391-nm lasing intensity from ionized nitrogen molecules in 800-nm femtosecond laser fields. Phys. Rev. A **97**, 033409 (2018). URL <https://link.aps.org/doi/10.1103/PhysRevA.97.033409>.
38. Arissian, L., Kamer, B., Rastegari, A., Villeneuve, D. M. & Diels, J.-C. Transient gain from N_2^+ in light filaments. Phys. Rev. A **98**, 053438 (2018). URL <https://link.aps.org/doi/10.1103/PhysRevA.98.053438>.
39. Britton, M. et al. Short- and long-term gain dynamics in N_2^+ air lasing. Phys. Rev. A **100**, 013406 (2019). URL <https://link.aps.org/doi/10.1103/PhysRevA.100.013406>.
40. Li, H. et al. Air lasing from singly ionized N_2 driven by bicircular two-color fields. Phys. Rev. A **99**, 053413 (2019). URL <https://link.aps.org/doi/10.1103/PhysRevA.99.053413>.
41. Ando, T. et al. Rotational, vibrational, and electronic modulations in N_2^+ lasing at 391 nm: Evidence of coherent $B^2\Sigma_u^+ - X^2\Sigma_g^+ - A^2\Pi_u$ coupling. Phys. Rev. Lett. **123**, 203201 (2019). URL <https://link.aps.org/doi/10.1103/PhysRevLett.123.203201>.
42. Li, H. et al. Significant enhancement of N_2^+ lasing by polarization-modulated ultrashort laser pulses. Phys. Rev. Lett. **122**, 013202 (2019). URL <https://link.aps.org/doi/10.1103/PhysRevLett.122.013202>.

REFERENCES

REFERENCES

43. Zhang, A. et al. Coherent modulation of superradiance from nitrogen ions pumped with femtosecond pulses. Opt. Express **27**, 12638–12646 (2019). URL <http://www.opticsexpress.org/abstract.cfm?URI=oe-27-9-12638>.
44. Zhang, A. et al. Subfemtosecond-resolved modulation of superfluorescence from ionized nitrogen molecules by 800-nm femtosecond laser pulses. Opt. Express **27**, 14922–14930 (2019). URL <http://www.opticsexpress.org/abstract.cfm?URI=oe-27-10-14922>.
45. Zhang, Q. et al. Sub-cycle coherent control of ionic dynamics via transient ionization injection (2019). arXiv:1911.01563.
46. Seideman, T. Revival structure of aligned rotational wave packets. Phys. Rev. Lett. **83**, 4971–4974 (1999). URL <https://link.aps.org/doi/10.1103/PhysRevLett.83.4971>.
47. Dooley, P. W. et al. Direct imaging of rotational wave-packet dynamics of diatomic molecules. Phys. Rev. A **68**, 023406 (2003). URL <https://link.aps.org/doi/10.1103/PhysRevA.68.023406>.
48. Popov, A. K. & Slabko, V. V. Inversionless amplification by anisotropic molecules. Opt. Lett. **30**, 1719–1721 (2005). URL <http://ol.osa.org/abstract.cfm?URI=ol-30-13-1719>.

REFERENCES

REFERENCES

49. Spanner, M. & Patchkovskii, S. One-electron ionization of multielectron systems in strong nonresonant laser fields. Phys. Rev. A **80**, 063411 (2009). URL <https://link.aps.org/doi/10.1103/PhysRevA.80.063411>.
50. Zhang, Y., Lötstedt, E. & Yamanouchi, K. Mechanism of population inversion in laser-driven N_2^+ . Journal of Physics B: Atomic, Molecular and Optical Physics **52**, 055401 (2019). URL <https://doi.org/10.1088%2F1361-6455%2Faafdbc>.
51. Gaarde, M. B. & Couairon, A. Intensity spikes in laser filamentation: Diagnostics and application. Phys. Rev. Lett. **103**, 043901 (2009). URL <https://link.aps.org/doi/10.1103/PhysRevLett.103.043901>.
52. Mitryukovskiy, S. I., Liu, Y., Houard, A. & Mysyrowicz, A. Re-evaluation of the peak intensity inside a femtosecond laser filament in air. Journal of Physics B: Atomic, Molecular and Optical Physics **48**, 094003 (2015). URL <https://doi.org/10.1088%2F0953-4075%2F48%2F9%2F094003>.